7) Variable features, when compared to Mariner 9 pictures taken 4 years ago, show relatively little change.

8) Several types of clouds were observed, including diffuse morning hazes in the northern hemisphere, discrete equatorial white clouds, and extensive wave clouds.

9) A direct measurement of wind velocity from cloud motion was achieved for the first time.

MICHAEL H. CARR
U.S. Geological Survey, Menlo Park, California 94025
HAROLD MASURSKY
U.S. Geological Survey, Flagstaff, Arizona 86001
WILLIAM A. BAUM
Lowell Observatory, Flagstaff, Arizona 86001
KARL R. BLASIUS
Science Applications, Inc., Pasadena, California 91101
GEOFFREY A. BRIGGS
Jet Propulsion Laboratory, Pasadena, California 91103
JAMES A. CUTTS
Science Applications, Inc., Pasadena
THOMAS DUXBURY
Jet Propulsion Laboratory, Pasadena
RONALD GREELEY
University of Santa Clara, Santa Clara, California 95053
JOHN E. GUEST
University of London Observatory, London, NW72QS, England
BRADFORD A. SMITH
University of Arizona, Tucson 85721
LAURENCE A. SODERBLOM
U.S. Geological Survey, Flagstaff
JOSEPH VEVERKA
Cornell University, Ithaca, New York 14853
JOHN B. WELLMAN
Jet Propulsion Laboratory, Pasadena

References and Notes

1. J. B. Wellman, F. P. Landauer, D. D. Norris, T. E. Thorpe, *J. Spacecraft Rockets*, in press; T. E. Thorpe, *Icarus* **27**, 229 (1976).
2. L. Tyler, personal communication.
3. D. H. Wilhelms, *U.S. Geol. Surv.* (1976), p. I-895; H. Masursky, N. J. Trask, M. E. Strobell, A. L. Dial, G. W. Colton, *U.S. Geol. Surv. Map*, in press; D. Milton, *U. S. Geol. Surv.* (1974), p. I-894.
4. M. H. Carr, H. Masursky, R. S. Saunders, *J. Geophys. Res.* **78**, 4031 (1973); D. Scott, *U.S. Geol. Surv.*, in press.
5. L. A. Soderblum, T. J. Kreidler, H. Masursky, *J. Geophys. Res.* **78**, 4117 (1973).
6. R. P. Sharp, *ibid.*, p. 4073.
7. M. Malin, thesis, California Institute of Technology (1976).
8. B. C. Murray, L. A. Soderblum, R. P. Sharp, J. A. Cutts, *J. Geophys. Res.* **76**, 313 (1971).
9. D. E. Wilhelms, *ibid.* **79**, 3933 (1974).
10. D. E. Gault, J. E. Guest, J. B. Murray, D. Dzurisin, M. Malin, *ibid.* **80**, 2444 (1975).
11. Variable features were first defined during the Mariner 9 mission to mean surface albedo patterns which changed with time; the term has since been used to include all surface forms that are commonly attributed to aeolian or wind processes [C. Sagan *et al., J. Geophys. Res.* **78**, 4163 (1973)].
12. C. B. Leovy *et al., ibid.*, p. 4252.
13. J. B. Pollack, C. B. Leovy, Y. Mintz, W. Van Camp, *Geophys. Res. Lett.*, in press; P. W. Webster, in preparation.
14. J. A. Pirraglia, *Icarus* **27**, 517 (1976).
15. We thank the following people for their untiring help during the early hectic stages of this mission: J. Boyce, P. S. Butterworth, K. W. Farrell, E. A. Flinn, H. Ferguson, A. Jankevics, K. P. Kaasen, C. Leavy, B. Lucchitta, J. MacQueen, T. E. Poe, Jr., G. Schaber, A. Spruck, E. E. Theiling, D. T. Thompson, and T. E. Thorpe. Financial support for the work of team members was provided by NASA Viking Project Office, NASA Office of Planetary Geology (R.G.), and U.K. Natural Environment Research Council (J.E.G.).

26 July 1976

Viking: Mars Atmospheric Water Vapor Mapping Experiment—Preliminary Report of Results

Abstract. *Observations made from the Viking 1 orbiter show very little water vapor in the Mars atmosphere in the southern hemisphere (0 to 3 precipitable micrometers) with a gradual increase across the equator to northern latitudes. Maximum amounts between 20 and 30 micrometers have been observed in the short period covered by the observations to date. The season, northern midsummer, corresponds to the beginning of the water vapor cycle in that hemisphere. A strong repetitive diurnal cycling between the solid and vapor phases is observed at a site to the east of the Tharsis Ridge at 10° north latitude; the vapor lies close to the martian surface and is most probably in saturation equilibrium with a surface haze or fog throughout much of the day.*

The water vapor mapping experiment is designed to determine the variability of the martian atmospheric vapor over a wide range of spatial and temporal scales. In order to separate the effects of spatial (global and vertical) and time-dependent (diurnal, seasonal, and perhaps longer-term) characteristics, the study must take advantage of the maximum flexibility available from the orbital coverage of the planet, particularly in securing nonsynchronous observation periods (*1*) and continuing through the seasonal progression obtainable from the Viking extended mission. Many of the characteristics of the martian water vapor, and especially those related to its variability, have been indicated by the behavior observed from Earth-based measurements (*2, 3*), and the strategy for the present Viking orbital study is based in large part on a model for the interaction between the planet's atmosphere and surface or subsurface material which the past observations have suggested. Thus, one of the principal objectives of the Viking measurements is to refine or revise this model; in this context, the present report must be of a very preliminary nature, since only a very restricted set of measurements made over a relatively short time span from synchronous orbit has been possible so far. The period covered is from approach [Mars orbit insertion (MOI) − 2 days] through Viking 1 lander separation (rev 30), during which emphasis has of necessity been placed on observations related to the characterization of the landing sites. Therefore, many of the water vapor mapping observation sequences necessary for the investigation as a whole have not yet been initiated.

It is pertinent at the outset to comment on the timing of the measurements reported here with respect to the seasonal variation of martian water vapor. Orbit insertion occurred (19 June 1976) when the planetocentric longitude (L_S) of Mars was 84° (L_S = 90° corresponds to the northern summer solstice). The accumulation of data from Earth-based observations has revealed a seasonal variation, the appearance of the vapor coinciding approximately with midsummer in each respective hemisphere and the maximum being reached some 2 months later. (The period of high vapor content and the time interval between the solstice and the maximum atmospheric vapor abundance are longer in the south than in the north.) Maximum values of about 50 precipitable micrometers (pr μm) averaged over a horizontal scale of ~ 10^3 km have been observed for both hemispheres, with the maximum apparently occurring at temperate latitudes. Against this framework, the present observations have been made at the onset of the northern "wet" season, and have so far covered the southern (dry) hemisphere and northern latitudes to about 20°, with a few isolated afternoon measurements in the latitude band 40° to 50°.

Instrument and observations. The instrument, the Mars atmospheric water detector (MAWD), is a grating spectrometer operating in the 7200 cm^{-1} (1.4 μm) water vapor bands. Absorption by the atmospheric vapor of solar radiation diffusely reflected from the surface of the planet is measured by five radiatively cooled PbS detectors located in the exit focal plane of the instrument. The detectors are arranged so that, when the grating is in its nominal "locked" position, their locations correspond to the wavelengths of three relatively strong absorption features close to the band center, and two "window" regions which can be used to define the local continuum. The spectral resolution of the instrument, 1.2 cm^{-1}, allows a detection capability of < 1 μm, under average to good conditions of the observation geometry. A brief description of the instrument and a discussion of the choice of spectral region and channel frequencies has been given by Farmer and LaPorte (*4*).

Because the three line channels (at 7223.13, 7232.20, and 7242.74 cm^{-1}) span a range of transition intensities of more than an order of magnitude, the three independent values of absorption measured at each position of the instrument field of view on the planet's surface can be used to determine the total atmospheric pressure and temperature at the level at which the bulk of the vapor resides. These values, in turn, provide an indication of the height of the vapor above the surface. It should be pointed out, however, that under martian conditions all three lines are in the saturated region of their curves of growth and therefore such simultaneous solutions for column abundance (W), pressure (P), and temperature (T) can only be satisfactorily obtained under the most favorable conditions (that is, line of sight abundance > 30 pr μm and incidence and emission angles $< 60°$).

Most of the planetary data are taken with the instrument operating in the "locked-up" mode, that is, with the grating position servo fixed at the nominal line and continuum center frequencies. A second mode of operation is available in which the grating is scanned over a small angular range (corresponding to a frequency range of $\pm$ 8 cm^{-1} about each channel center frequency) to provide continuous spectral coverage of the region between 7215 and 7251 cm^{-1}. Instrument operation in the wavelength scanning mode is included occasionally in the observation sequences in order to monitor the spectral resolution of the five channels together with a number of other instrument functional parameters, and (initially) to verify the spectral details assumed for martian atmospheric conditions in the design of the instrument and the data reduction software.

The angular size of the instantaneous field of view (IFOV) of MAWD is 2×16 mrad, which corresponds to a spatial resolution of 3×24 km on the surface at a periapsis altitude of 1500 km. This field is

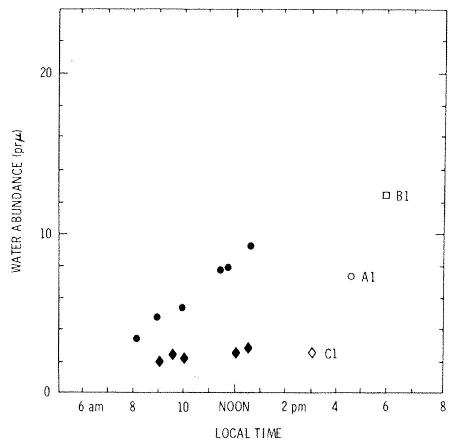

Fig. 1. Diurnal behavior of martian water vapor at three sites: (●) 10°,83° and (◆) −15°,69° and −17°,77°.

stepped sideways by increments equal to the short dimension to provide a raster consisting of 15 contiguous elements covering a total area of ~ 20×45 km (at periapsis). The signal integration time for each IFOV is 0.28 second, so that the raster scan time, including flyback, is 4.48 seconds. The raster pattern is used in conjunction with the scan platform motion in the design of the individual observation sequences to provide the variety of low-resolution (high-altitude) and high-resolution coverages needed to carry out the vapor mapping investigation.

The data reduction and analysis programs are designed to enable the three parameters W, P, and T to be determined from the five measured channel radiances at the IFOV spatial scale, or from radiance averages taken over larger areas corresponding to one or more complete rasters. The extraction of water vapor data at degraded spatial resolution is important in that measurements can be made under conditions of greatly reduced illumination (for example, close to the morning and evening terminators) and which would otherwise be unreliable at the IFOV scale. This aspect has been of significance in the data taken so far because of the emphasis which has been placed on characterization of the landing sites: from the present synchronous orbit the accessible sites at all three candidate site latitudes (− 5°, 20°, and 44°) can only be viewed at local times within 1 or 2 hours of sunrise or sunset—indeed the solar elevation angle at the 44° prime site for the Viking 2 lander at the time of overflight of the Viking 1 orbiter is $< 10°$, and the corresponding signal radiance more than an order of magnitude lower than that required for reliable vapor abundance measurements at the highest (IFOV) spatial resolution. Thus, averaging over the area of some tens of rasters was necessary for the reduction of the B site data.

Approach observations. Several observations of Mars were obtained before orbit insertion. While intended primarily to be instrument performance checks, these approach observations allowed us to see, albeit at poor resolution, regions of the planet that are inaccessible from the Viking 1 synchronous orbit. Viking 1 approached Mars from the morning side, so the amounts of water measured on approach refer to midmorning abundances. In general, where comparison with later orbital observations was possible, the results were consistent.

Approach observations of areas not observed during orbital operations showed abundances similar to those obtained at about 90° west longitude from orbit, with a couple of notable exceptions. The approach observations of the Hellas–Sinus Sabaeus area, about 310° west, show three to four times as much water vapor as at points at corresponding latitudes on the planet. The other exception is the Elysium-Amazionis region, where we measure 30 μm, the largest abundance we have observed to date anywhere on the planet. We hope to be able to confirm the latter measurements later in the mission when we are able to observe the planet from an asynchronous orbit.

Diurnal behavior. One of the most powerful observational clues to the water cycle on Mars is the behavior of the abundance of water vapor at a particular location from sunrise to sunset. Very little water vapor can be retained in the vapor phase at low altitudes during the cold martian night; how rapidly it returns from the solid to the vapor phase when the ground and atmosphere start to warm up in the morning is controlled by whether the ice is on the surface, diffused into the soil, or suspended in the low atmosphere. When, and how rapidly, it returns to the solid phase as the atmosphere cools off in the afternoon and evening is controlled by how far up in the atmosphere the vapor manages to mix during the day.

In order to view a particular site at several local times in both the morning and evening, it is necessary to be in an asynchronous orbit. During the site certification time period the orbit was synchronized over the nominal A1 landing site, and we were therefore only able to get partial diurnal behavior at any particular location on the planet. We monitored three sites at coordinates (latitude, longitude) of 10°,83°; − 15°,69°; and − 17°,77° from dawn to local noon. The 10°,83° site was chosen because it was the site closest in latitude and elevation to the A1 site which could be observed for an extended period of time; the second two were chosen because of their similiarity to the C1 site. None of the actual sites A1, B1, or C1 could be observed for an extended period of time from the Viking 1 synchronous orbit.

Figure 1 shows the diurnal behavior of the water vapor in the three areas, with the A1, B1, and C1 periapsis observations included for reference. The two C-site analogs had identical diurnal behavior; this, together with their topographical similarity to C1, leads us to believe that these southern areas are very

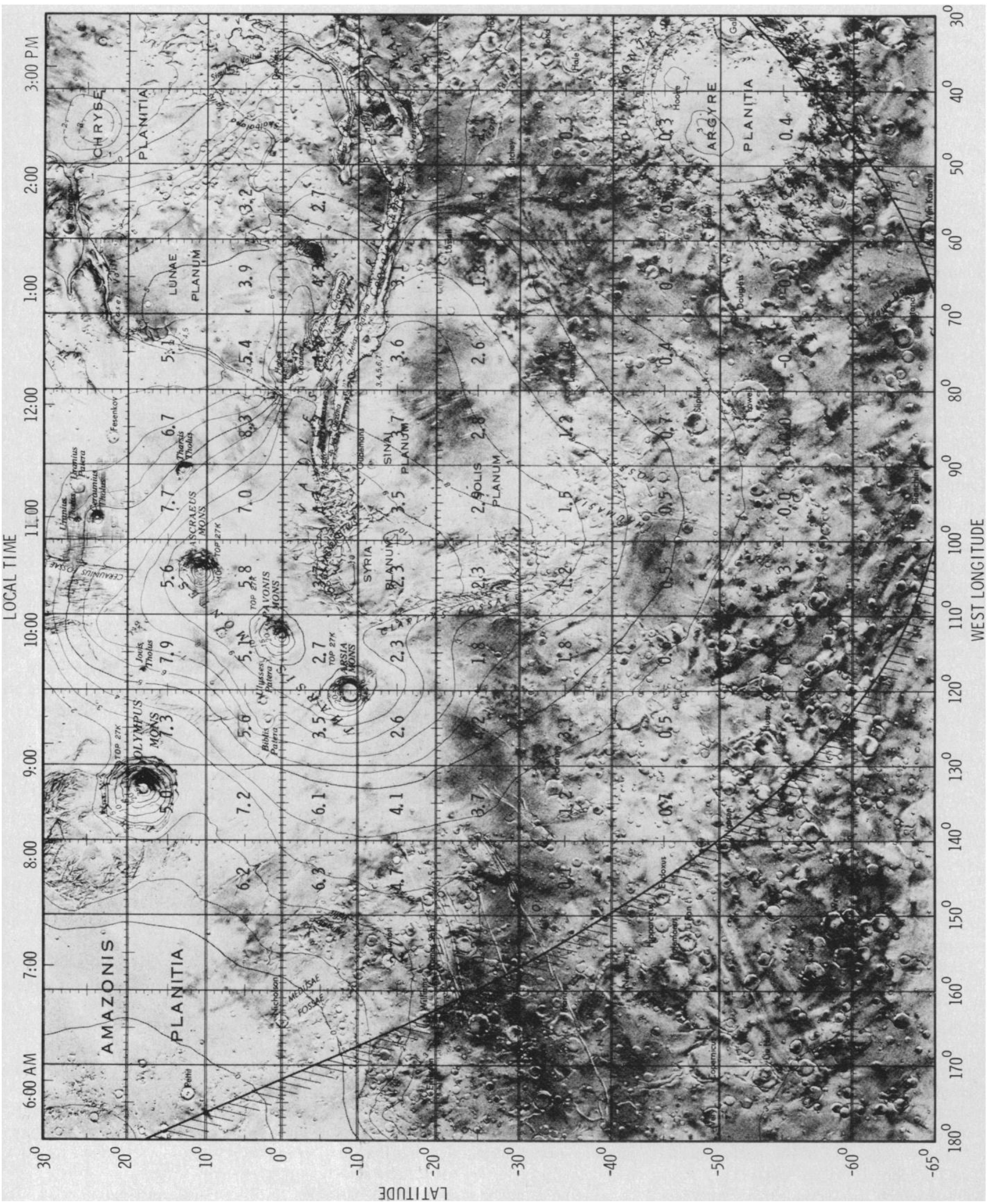

Fig. 2. Low-resolution map of total atmospheric vapor content (precipitable micrometers) from observations made approximately 1.5 hours before periapsis on revs 6 to 9, 12, and 13. The crosshatched line represents the position of the terminator.

similar in behavior, and that the composite diurnal behavior displayed by them is typical of the region just south of the equator in the vicinity of Valles Marineris at this season.

We do not expect 10°,83° to be a very good analog of the A1 site. The two areas are in different geologic regions, and the 10°,83° area is about 5 km higher. Therefore, it is not safe to assume that 10°,83° and A1 display the same diurnal behavior. Further comments on the inferences to be drawn from the diurnal behavior are given in the discussion below.

Low-resolution mapping. During the first 13 orbits, box scans were made of the planet at various times from periapsis. In general, the Viking 1 orbit allows extended observation sequences of the morning areas of the planet only; the afternoon and evening regions are overflown very quickly right at periapsis. The most extensive series of observations were made about 90 minutes before periapsis, while the spacecraft was viewing the region south of and including Tharsis and Valles Marineris. Figure 2 is a map of water abundance obtained by combining the results obtained from the high-altitude scans made on revs 6 to 9, 12, and 13. Also included for reference are the terminator (morning terminator on the left side) and the local time.

The most striking feature of the map is the strong latitude dependence of the water vapor abundance. Near the south polar cap we find < 0.5 pr μm; this value increases almost linearly with decreasing latitude across the equator to 20°, the northern limit of the observations. In Fig. 3 we have displayed the latitude dependence of the average vapor content between longitudes corresponding to 0930 and 1330 hours local time.

In the equatorial and northern latitudes shown in Fig. 2, the early morning longitudes show as much water vapor as the longitudes observed at local noon. If all sites displayed the same diurnal behavior as the 10°,83° site, we would expect to see an increase in vapor abundance from the morning terminator to noon; since this is clearly not the case, we must conclude that there are significant differences in the behavior of water vapor at different areas of the planet. In particular, compared to 10°,83°, the region to the west of Tharsis either reaches its maximum much earlier in the day or, if it has the same gradual buildup of vapor, must reach a value of some 15 to 20 μm by noon. In the latter case it is interesting to note (as mentioned in the section on approach observations) that the region about 70° west of Tharsis showed

Table 1. Comparison of landing sites.

Site	Latitude	Longitude	Local time (hours)	Water vapor abundance (pr μm)
A1	20°	30°	1620	7.3 ± 1.2
B1	45°	10°	1800	12.4 ± 3.8
C1	−5°	45°	1530	2.7 ± 0.8

the largest amounts of water vapor we have so far observed. Selection between the two hypotheses will have to await observations from asynchronous orbit.

There is an indication from the map of an anticorrelation between elevation and water abundance in the area of the Tharsis Ridge. Measurements taken over Tharsis tend to be 20 to 50 percent lower than those over adjacent areas to the east and west. Part of this effect is due to the method of calculation used in these preliminary data. The calculated water abundance depends on the effective pressure assumed for the vapor. For the data presented in this report we have assumed a pressure of 6 mbar independent of location. If a lower pressure had been used, the calculated amount of water would have been higher—a 5-km change in elevation would produce a 25 percent change in water abundance, fairly close to the observed decrease over the Tharsis area.

Landing site comparison. As part of the site certification process for Viking 1, measurements of the water vapor over the original A1 site were obtained on revs 3 to 7. In order to help determine the latitude for the Viking 2 lander, observations were also made of two potential sites for Viking 2. Table 1 gives the relevant data for the three sites A1, B1, and C1. Errors quoted are 1 standard deviation. The A and C site data show the same trend of increasing water abundance to the north as the global map; the

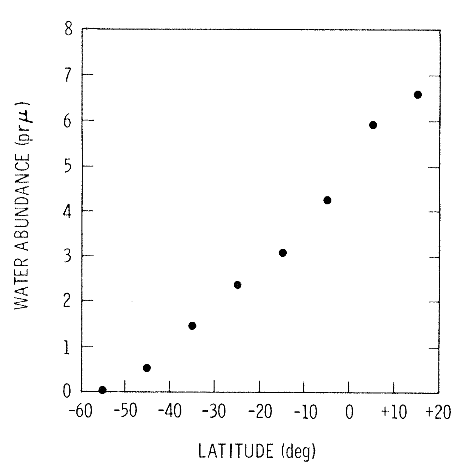

Fig. 3. Mean latitude dependence of water vapor between 0930 and 1330 hours local time.

B site data indicate that the trend continues at least as far north as 45°. Since the B site is observed much closer to the evening terminator than the C site, and since it is hard to imagine a situation where the abundance would be increasing with time near dusk, lack of knowledge of the diurnal behavior in the late afternoon does not affect the conclusion that the B site has far more atmospheric water vapor during the day than does the C site.

Discussion. The linear character and repeatability of the growth of vapor at the diurnal site suggest that, at this location and season at least, the vapor is contained within the atmospheric layer closest to the surface. Although the local time at which the maximum of this daily cycle is reached is not observed in the data, it is clear that at least 80 percent of the vapor returns to the solid phase at some time between noon and the following dawn. The low altitude of the vapor on a planetwide scale at the time of maximum vapor abundance had been suspected from the results of Earth-based spectroscopy (*5*), which gave a rotational temperature for the water vapor (225°K) higher than that of the bulk atmosphere (204°K). In the present instance, the low altitude of the vapor is inferred from the fact that the only region of the atmosphere which undergoes sufficient diurnal temperature excursions (*6*) to cause the condensation and reevaporation of the measured quantities of vapor is the boundary layer—that is, the layer whose temperature is closely coupled to the temperature of the surface.

The sublimation of a layer of *exposed* ice deposited on the surface must be discarded as the direct source of the vapor observed at the diurnal site, because its lifetime in the solid phase at dawn would be too short to give the observed slow increase in vapor. For example, the insolation on a horizontal surface 1 hour after sunrise (4×10^{-3} cal cm^{-2} sec^{-1}) is equivalent to the latent heat of vaporization of 2×10^{17} mol cm^{-2} sec^{-1} of ice (assuming an albedo of 0.9), so that the lifetime of 10 μm of frost under these conditions would be about 5 minutes. The rapid evaporation of the surface frost at sunrise could, however, be the initial source of a ground fog, whose subsequent evaporation would produce the observed increase of vapor. The diurnal variation of vapor from exposed surface ice which does *not* pass through a second condensation phase to form an atmospheric haze layer would characteristically reach a maximum very early in the day, and this behavior may explain the trend observed in Fig. 2 for the region to the west of Tharsis mentioned earlier.

The presence of a ground fog is not unexpected, and has been discussed in recent papers by Flasar and Goody (*7*), Hess (*8*), and Farmer (*3*). While this is a possible explanation for the observed diurnal behavior (at 10°,83°), we cannot at present entirely rule out the release of vapor from ice entrained in the topmost layer of the regolith material, or the gradual reduction of opacity of a higher-elevation cloud layer above the vapor, as possible alternate explanations. Unfortunately, we have not yet obtained any high-altitude images of this area to aid in the interpretation of the data.

A further inference can be drawn from the fact that, since the vapor is still increasing at the time of the last diurnal observation, ~1300 hours, it is reasonable to assume that there is still some condensate in the atmosphere or near-surface layer at that time. This result suggests that some fraction of the water remains in the solid phase throughout the day; one interpretation of the latitude–time of day trend shown in Fig. 2 is that this fraction increases toward the northern midlatitudes. Hence we might expect that, as the northern summer progresses, the lower latitude limit of the atmospheric condensate layers will recede, with a corresponding increase in the fractional amount of ice vaporized during the day, and a decrease in the amplitude of the diurnal vapor cycle as the vapor becomes mixed into the bulk atmosphere above the boundary layer trap. At this stage the meridional circulation will carry the vapor to the cooler latitudes (principally the winter hemisphere).

The Viking 1 orbital observations conveniently cover the period of the northern water vapor growth and decay, and the second spacecraft (Viking 2 orbiter) will give good polar coverage of the latter stages of this phase. The extended mission, with both spacecraft, will enable the progression of the seasonal cycle into the southern hemisphere to be followed. The mission plans for the orbiters thus present an excellent opportunity during the forthcoming months to study the variability of the vapor and its interaction with the surface of the planet over a wide range of spatial and temporal scales, and to test the validity of some of the theories which have been proposed to explain its cyclic behavior.

CROFTON B. FARMER
DONALD W. DAVIES
Jet Propulsion Laboratory, California Institute of Technology, Pasadena 91103
DANIEL D. LAPORTE
Santa Barbara Research Center, Goleta, California 93017

References and Notes

1. For a discussion of the orbit geometry and the corresponding opportunities for observational coverage, see G. A. Soffen and C. W. Snyder, *Science* **193**, 759 (1976).
2. See E. S. Barker, *Icarus* **28**, 247 (1976), and references contained therein.
3. C. B. Farmer, *ibid.*, p. 279.
4. ______ and D. D. LaPorte, *ibid.* **16**, 34 (1972).
5. R. A. Schorn *et al.*, *ibid.* **11**, 283 (1969); R. G. Tull, *ibid.* **13**, 43 (1970).
6. Day and night vertical profiles of temperature for this region of the planet at this season were obtained from Mariner 9 (IRIS); see B. Conrath *et al.*, *J. Geophys. Res.* **78**, 4267 (1973). The expected small variation in the diurnal temperature extremes for the bulk atmosphere above the boundary layer was first discussed by P. Gierasch and R. Goody, *Planet. Space Sci.* **16**, 615 (1968).
7. F. M. Flasar and R. M. Goody, *Planet. Space Sci.* **24**, 161 (1976).
8. S. L. Hess, *Icarus* **28**, 269 (1976).
9. A large number of people have contributed to the design and construction of the flight instruments, which have operated flawlessly, and to the development of the special-purpose computer and its software system used for the data analysis. We are grateful to all of these, whose enthusiastic involvement has ensured the success of the experiment. We thank especially W. Carls, H. Clark, J. Geiselman, E. Goldyn, S. Hanson, A. Holland, R. Kares, R. Killian, D. Langford, F. Murphy, J. Riccio, and D. Rupnik for their considerable efforts over the past months: this is submitted on their behalf. This report presents the results of one phase of research carried out at the Jet Propulsion Laboratory under NASA contract NAS 7-100.

26 July 1976

Infrared Thermal Mapping of the Martian Surface and Atmosphere: First Results

Abstract. *The Viking infrared thermal mapper measures the thermal emission of the martian surface and atmosphere and the total reflected sunlight. With the high resolution and dense coverage being achieved, planetwide thermal structure is apparent at large and small scales. The thermal behavior of the best-observed areas, the landing sites, cannot be explained by simple homogeneous models. The data contain clear indications for the relevance of additional factors such as detailed surface texture and the occurrence of clouds. Areas in the polar night have temperatures distinctly lower than the CO_2 condensation point at the surface pressure. This observation implies that the annual atmospheric condensation is less than previously assumed and that either thick CO_2 clouds exist at the 20-kilometer level or that the polar atmosphere is locally enriched by noncondensable gases.*

Experiment description. The Viking infrared thermal mapper (IRTM) contains four telescopes, each with seven detectors. Thermal emission from the planet's surface is measured in four bands, 6.1 to 8.3, 8.3 to 9.8, 9.8 to 12.5, and 17.7 to 24 μm; there are three detectors in each of the first two bands and seven in each of the last two. One detector at 14.56 to 15.41 μm, centered on the CO_2 vibration band, measures the stratospheric temperature. Brightness temperatures in these bands are identified as T_7, T_9, T_{11}, T_{20}, and T_{15}. Seven detectors at 0.3 to 3.0 μm respond to reflected sunlight.

An objective of this investigation was to achieve good spatial resolution. The field of view is defined by focal plane stops 5.2 mrad in diameter. The spatial response has been measured in the laboratory and verified in flight to be nearly diffraction-limited. In the longest wavelength band, the signal at the planetary limb drops to 10 and 1 percent of maximum when the limb is at distances of 6 and 17 mrad from the center of the field of view. The radiation level is integrated in all channels simultaneously; this arrangement allows measurements of the brightness temperatures and the reflected radiance at seven locations on the planet each 1.12 seconds.

The response of all channels is nearly linear with flux, and is digitized into 1000 data numbers (DN). The maximum response of the solar band corresponds to 75 percent of a perfect white diffuser at normal incidence at the mean Mars distance from the sun. The thermal bands have maximum temperatures between 300 and 330 K. The one-sample noise is less than 1 DN for all channels except T_{15}, where it is about 2.5 DN. The equivalent temperature uncertainty varies with band and temperature; the 7- and 9-μm bands are well on the short wavelength side of the Planck function at 200 K, and only the 20-μm band has good temperature resolution below 170 K.

The angular resolution, detector configuration, sample rate, and scan-platform slew rate were designed to allow approximately uniformly spaced, nonredundant, continuous coverage so that the IRTM experiment can produce two-dimensional images in the solar and thermal bands (*1*). The in-flight performance of the IRTM has been entirely as expected, including some sensitivity to thermal radiation from the Viking lander prior to separation. The results reported here were obtained on revolutions (revs) 3 through 22, occurring over 22 June to 11 July 1976.

Global surface temperatures. From apoapsis to approximately 2 hours before periapsis the entire disk of Mars can be scanned in a single observation se-